

Geophysical Research Letters

RESEARCH LETTER

10.1029/2019GL085167

Key Points:

- Hydraulic fracturing induced ~90 earthquakes larger than magnitude 2.0 in the Eagle Ford shale play of south Texas from 2014–2018
- One of the largest events potentially induced by hydraulic fracturing in the US occurred near the largest recorded event in south Texas
- We propose hydraulic fracturing of multiple laterals simultaneously increases the probability of earthquakes relative to wells in isolation

Supporting Information:

- Supporting Information S1
- Data Set S1

Correspondence to:

S. L. Fasola,
fasolasl@miamioh.edu

Citation:

Fasola, S. L., Brudzinski, M. R., Skoumal, R. J., Langenkamp, T., Currie, B. S., & Smart, K. J. (2019). Hydraulic fracture injection strategy influences the probability of earthquakes in the Eagle Ford shale play of South Texas. *Geophysical Research Letters*, 46, 12,958–12,967. <https://doi.org/10.1029/2019GL085167>

Received 27 AUG 2019

Accepted 9 NOV 2019

Accepted article online 13 NOV 2019

Published online 27 NOV 2019

Hydraulic Fracture Injection Strategy Influences the Probability of Earthquakes in the Eagle Ford Shale Play of South Texas

Shannon L. Fasola¹ , Michael R. Brudzinski¹ , Robert J. Skoumal² , Teresa Langenkamp¹ , Brian S. Currie¹ , and Kevin J. Smart³ 

¹Department of Geology and Environmental Earth Science, Miami University, Oxford, OH, USA, ²U.S. Geological Survey, Earthquake Science Center, Menlo Park, CA, USA, ³Earth Science Section, Southwest Research Institute, San Antonio, TX, USA

Abstract Seismicity in the Eagle Ford play grew to 33 times the background rate in 2018. We identified how hydraulic fracturing (HF) contributed to seismicity since 2014 by comparing times and locations of HF with a catalog of seismicity extended with template matching. We found 94 $M_L \geq 2.0$ earthquakes spatiotemporally correlated to 211 HF well laterals. Injected volume and number of laterals on a pad influence the probability of seismicity, but effective injection rate has the strongest effect. Simultaneous stimulation of multiple laterals tripled the probability of seismicity relative to a single, isolated lateral. The 1 May 2018 $M_w 4.0$ earthquake may have been the largest HF-induced earthquake in the United States. It occurred ~10 km from a $M_w 4.8$ earthquake in 2011 and was thought to be induced by fluid extraction. Thus, faults in this area are capable of producing felt and potentially damaging earthquakes due to operational activities.

Plain Language Summary We investigated the recent increase in seismicity rate in the Eagle Ford oil and gas field of south Texas in 2018 that grew to 33 times higher than previous years and how hydraulic fracturing (HF) contributed. We compared times and locations of HF wells with a catalog of seismicity we enhanced through seismogram similarity detection. Over 200 HF wells had seismicity nearby during operation with ~90 earthquakes having magnitudes ≥ 2.0 , indicating seismicity from HF is more common in this area than previously thought. We found that HF strategy affects the probability of earthquakes. Seismicity was twice as likely when operators inject into multiple nearby wells simultaneously compared to when they inject into multiple wells one at a time. The simultaneous strategy was three times more likely to produce seismicity compared to a single well strategy. Of the ~2,400 HF-induced earthquakes we identified, a magnitude 4.0 is one of the largest reported in the United States, and it occurred ~10 km from the largest (magnitude 4.8) earthquake in south Texas, thought to be due to fluid extraction in 2011. This study demonstrates that faults in this area are capable of producing felt and potentially damaging earthquakes due to ongoing HF.

1. Introduction

The increased occurrence of earthquakes ($M_L \geq 3$) in central and eastern United States has mostly been attributed to the large volume injection of wastewater brines, coproduced during oil and gas extraction, into deep sedimentary layers (wastewater disposal [WD]; e.g., Ellsworth, 2013; Keranen et al., 2013; Walsh & Zoback, 2015; Weingarten et al., 2015). However, other human activities have been associated with the production of seismicity including hydraulic fracturing (HF; e.g., Skoumal et al., 2015), enhanced geothermal (e.g., Johnson, 2014), carbon sequestration (e.g., Kaven et al., 2015), and hydrocarbon/water extraction (e.g., Frohlich & Brunt, 2013). While microseismicity ($M_L < 1$) is an inherent component of rock-fracturing during HF (e.g., Warpinski et al., 2012), stimulations that induce larger magnitude events along preexisting faults (“HF-induced seismicity”) have become more common (e.g., Atkinson et al., 2016; Brudzinski & Kozlowska, 2019; Clarke et al., 2014; Farahbod et al., 2015; Lei et al., 2017, 2019; Schultz et al., 2017; Skoumal, Ries, et al., 2018; Yoon et al., 2017). Several studies suggest that HF poses a lower probability of producing felt events (typically $M_L \geq 3$) than WD due to the shorter duration (days to weeks for HF vs. months to years for WD) and lower total volumes of injection (e.g., National Research Council, 2013;

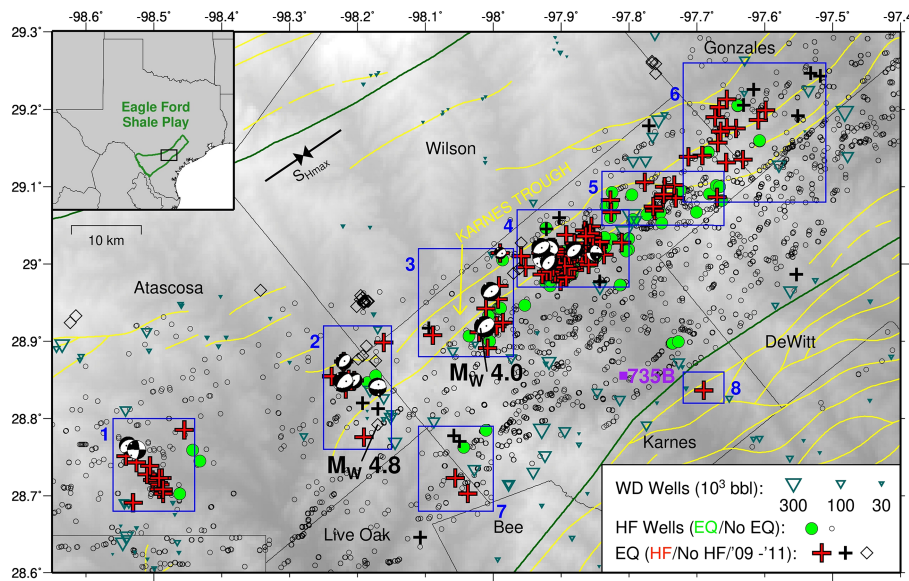


Figure 1. Map of study region in the Eagle Ford shale play of south Texas. Texas Seismological Network earthquakes analyzed in this study (crosses), with Texas Seismological Network focal mechanisms shown. HF wells are indicated by black circles (FracFocus). Correlated earthquakes and HF wells are red and green, respectively. Black diamonds show 2009–2011 earthquakes (Frohlich & Brunt, 2013). Purple square shows the seismic station (735B) used for template matching. WD wells are teal triangles sized by median monthly volumes. Arrows show regional S_{HMAX} (Lund Snee & Zoback, 2016). Numbered blue boxes outline our focus regions. Faults (Ewing, 1990) are in yellow. Grayscale background shows topography, and counties are outlined in black. HF = hydraulic fracturing, WD = wastewater disposal.

Rubinstein & Mahani, 2015). The largest magnitudes of documented HF-induced events, however, have increased recently to include a M_w 5.3 in China, which injured 17 people and caused large-scale landslides, extensive damage to ~400 houses, and a direct economic loss of ~\$7 million (Lei et al., 2019). This event magnitude is approaching the largest (M_w 5.8) WD-induced earthquake in Oklahoma (Walter et al., 2017; Yeck et al., 2017). The potential for these larger magnitude events to cause damage underscores the need to understand the causes of induced seismicity and influences of different operational strategies. Recent work has suggested that proximity of operations to seismogenic faults and the orientation of those faults in the regional stress field are key factors, but not all induced seismicity has occurred on optimally oriented faults (e.g., Haffener et al., 2018; Hennings et al., 2019; Pawley et al., 2018; Skoumal, Brudzinski, et al., 2018, 2019; Walsh & Zoback, 2016).

South Texas is an area of interest for studying induced seismicity, because it has a history of active oil and gas production, HF, WD, and seismicity; some of which occurs within or near areas of pervasive faulting (Figure 1; Ewing, 1990; Frohlich et al., 2016). With the advancements in horizontal drilling and HF, the Eagle Ford shale play (EF) has focused on hydrocarbon production of the Upper Cretaceous Eagle Ford Formation and the Austin Chalk Formation directly above since 2008 (Frohlich & Brunt, 2013; Martin et al., 2011; Pearson, 2012; RRC, 2019). Since 2012, the EF has produced the second largest amount of oil in the United States, averaging 1.3 million barrel per day (Energy Information Administration, 2019). EF seismicity has been largely attributed to increases in hydrocarbon production with a few cases related to WD since 1973 (Davis et al., 1995; Frohlich & Brunt, 2013; Frohlich & Davis, 2002; Olson & Frohlich, 1992; Pennington et al., 1986). There are no previously documented cases of HF-induced seismicity in the EF, but Walter et al. (2018) identified a few potential cases in the Texas Panhandle to the northwest of our study region.

In 2018, the rate of $M \geq 3.0$ earthquakes in the EF grew to 33 times higher than background levels (3 per 10 years from 1980–2010, Figure 2 inset). This study investigates seismicity since 2014 by examining how HF and WD may have contributed to the rate increase. A better understanding of the relationship between operations and seismicity has the potential to provide insight into the physical mechanisms of injection induced seismicity and specifically to help differentiate whether injected volume, injection rate, or

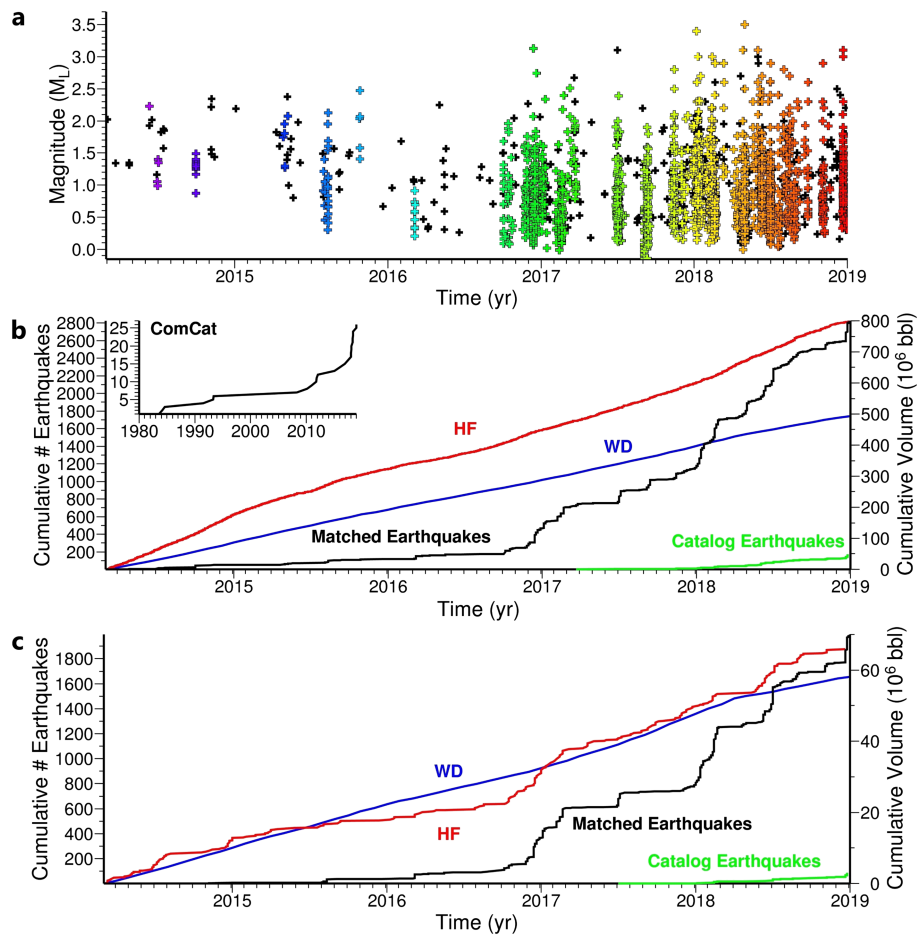


Figure 2. Number of earthquakes and injected volume over time. (a) Magnitude versus time for matched events. Earthquakes (crosses) that correlated with HF wells are colored, otherwise they are black. (b) Comparison of the cumulative HF (red: FracFocus) and WD (blue: RRC) cumulative injected volume, total matched earthquakes (black) and catalog template earthquakes (green: TexNet) for the entire study region. Inset shows cumulative number of earthquakes $M \geq 3.0$ from the Advanced National Seismic System comprehensive catalog (ComCat) since January 1980. (c) Same as (b) but for Region 4 only. HF = hydraulic fracturing, WD = wastewater disposal.

changes in injection rate are more responsible for seismogenesis (e.g., Chang et al., 2018; McGarr, 2014; Schultz et al., 2018; Segall & Lu, 2015; Weingarten et al., 2015). There is no traffic-light protocol in place for any type of induced seismicity in Texas to regulate operations as there is in other jurisdictions such as Ohio, Oklahoma, and Alberta (Alberta Energy Regulator, 2015; Ohio Department of Natural Resources, 2017; Oklahoma Corporation Commission, 2018). Identifying spatio-temporal relationships and driving factors between operational strategies and seismicity in the EF would help inform regulators and operators on strategies to best mitigate the seismic hazards.

2. Methods

Our analysis employs waveform cross-correlation (“template matching”) using the Texas Seismological Network (TexNet) catalog as earthquake templates to enhance the detection of seismicity and estimate magnitudes of smaller events (e.g., Schaff & Richards, 2014; Skoumal et al., 2014; Skoumal, Brudzinski, et al., 2018). There were 162 events in our study area since the TexNet catalog began in 2017, and we pursued template matching using a single nearby station (735B, UC San Diego, 2013) as other available stations (IRIS Transportable Array, 2003) proved too far away to be useful (see supporting information). Matched events were assigned the location of its best matched catalog template. We compared the improved seismicity catalog (supporting information, Data set S1) with the times and locations of HF from the FracFocus catalog, a

national hydraulic fracture chemical registry, and monthly volumes and locations of WD from the Texas Railroad Commission. We used the start and end times of well-lateral stimulation as detailed stimulation reports of individual stages were not publicly available. To investigate the cause of this seismicity, we followed the approach of previous work (Brudzinski & Kozłowska, 2019; Skoumal, Ries, et al., 2018) and divided the seismicity into eight regions ~20-km wide for detailed comparison with operational activity (Figures 1 and supporting information, S2). Earthquakes were correlated with HF wells if there were at least five earthquakes within 7 days of stimulation and within 10 km of active HF wells in all regions except Region 4 where we used a 5-km threshold due to additional stations that resulted in a lower location uncertainty and lower magnitude of completeness (see supporting information). For HF, we also evaluated the influence of operation strategy, target formation, injected volume, and number of wells per pad on the likelihood of seismicity using statistical modeling. For continuous data, logistic regression produced a probability curve that best fits the input data and calculates the *p* value for the probability the factor does not influence seismicity. For binary factors, we calculated an odds ratio to estimate the relative change in likelihood of seismicity and a corresponding *p* value test for significance (Altman, 1991; Sheskin, 2004). See supporting information for more details on our methods.

3. Spatial, Temporal, and Magnitude Distribution of Seismicity

While most cases of induced seismicity occurred along previously unmapped faults (e.g., Keranen & Weingarten, 2018), the earthquakes in our study area primarily occurred along mapped normal faults that trend NE/SW (Figure 1; Ewing, 1990). Template matching identified an additional 2,661 earthquakes from March 2014 through December 2018. About a quarter of the earthquakes occurred prior to the first cataloged earthquake in March 2017, indicating the usefulness of template matching for extending the seismicity catalog prior to when TexNet recording began in January 2017. The enhanced catalog of 2,823 earthquakes showed several short-lived, spatiotemporally clustered events (Figure 2a), characteristic of HF-induced seismicity (e.g., Kozłowska et al., 2018; Lei et al., 2017; Schultz et al., 2017; Skoumal, Ries, et al., 2018). These bursts of earthquakes, which we refer to as sequences, began in June 2014 and increased in prevalence during late 2016. We noticed there was a change in the maximum magnitude of events where up until November 2016; the largest events observed were a few M_L 2.0–2.5 earthquakes per year, but starting in December 2016 when there was also an increase in the number of sequences, the largest events increased to a few M_L 3.0–3.5 earthquakes per year (Figure 2a).

4. Correlations Between HF and Seismicity

Generally, we did not find a correlation between the temporal distribution of seismicity over the whole study region and the HF or WD injected volume (Figure 2b). However, we did find a correlation with HF when focusing on smaller regions. In Region 4 where 70% of the seismicity occurred, we identified a correlation between fluctuations in seismicity rate and the rate of HF (Figure 2c). There were notable increases in seismicity coincident with increases in the cumulative HF injected volume, while the cumulative WD injected volume showed a nearly constant slope. The WD injected volume per month nearly doubled in 2017, but this increase occurred after the jump in seismicity, and then dropped below the initial injection rate in 2018 while seismicity continued to increase. Our other focus regions showed a similar lack of spatiotemporal correlations between WD and seismicity (Figure S2). We also note that there are far fewer WD wells (~160) than HF wells (~4,300) in our overall study area, with few WD wells with injection rates exceeding 300,000 barrel per month (Figure 1). We cannot rule out that the gradual increase in cumulative WD volume during the study time period contributed to the seismicity, but the temporal correlation of HF wells and seismicity suggests HF was a more likely triggering mechanism.

We identified 211 HF wells (8%) from 80 well pads that correlated with 2,407 earthquakes (87%) within our eight focus regions (supporting information, Table S1). Overall, the proportion of earthquakes correlated with HF in our focus regions ranged from 60% to 100%, similar to that in the Appalachian Basin and Oklahoma (Brudzinski & Kozłowska, 2019; Skoumal, Ries, et al., 2018). The proportion of HF wells that correlated with seismicity in our focus regions was typically lower (2–7%) than those observed in previous studies of induced seismicity focus regions (~15%; Brudzinski & Kozłowska, 2019; Schultz et al., 2018; Skoumal, Ries, et al., 2018). We did observe higher percentages of HF wells with seismicity in Regions

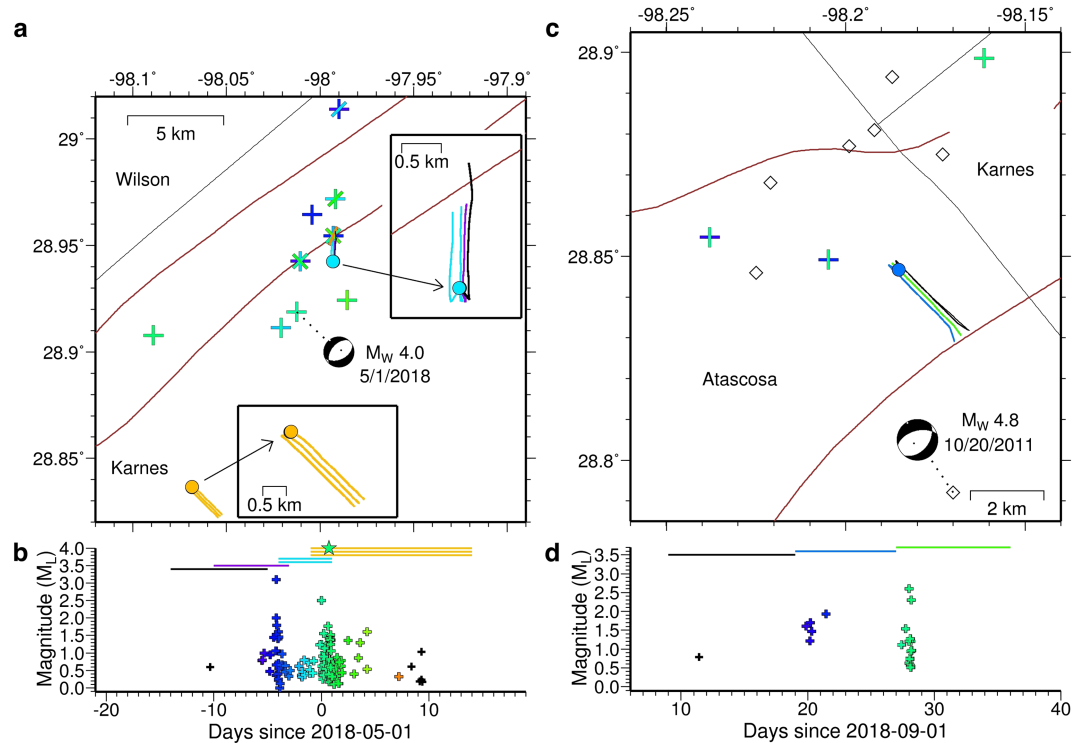


Figure 3. Examples of HF-induced seismicity from simultaneous lateral stimulation (a and b) and sequential lateral stimulation (c and d). (a) Map of a key sequence in Region 3 resulting in a M_W 4.0 (M_L 3.5) earthquake showing HF well pads (circles), digitized HF well laterals (lines: RRC), earthquakes (crosses), and focal mechanism (Texas Seismological Network). HF well pads, laterals, and seismicity are colored by time when correlated, otherwise they are black. Earthquakes have multiple colors if more than one HF well triggered that template earthquake over time. (b) Magnitude–time distribution for matched events (crosses). Reported HF times (FracFocus) are shown as thin lines at the top of the graph. (c) Map of September 2018 sequence in Region 2. Layout is similar to (a) but with 2009–2011 induced seismicity as black diamonds and the focal mechanism of the M_W 4.8 20 October 2011 earthquake (Frohlich & Brunt, 2013). (d) Magnitude–time distribution.

5 (13%) and 4 (32%), suggesting that the central portion of the southern bounding fault on the Karnes Trough is more prone to seismicity than other areas (Figure 1). We do not think this was an artifact of the relative distance from the seismic station as Region 3 (only 4% HF wells correlated) was closer than Region 5. We noted that ~10% of the HF wells in our eight focus regions targeted the Austin Chalk Formation (265 wells) rather than the Eagle Ford Formation (2,229 wells) where a lower percentage of wells correlated with seismicity (7.1% vs. 19.2%, supporting information, Table S2). The difference in earthquake probability appears to be a result of the geographic distribution of HF wells as the Austin Chalk is only targeted in a narrow zone where the seismicity was located (supporting information, Figure S7), supporting the widely held notion that proximity to susceptible faults is a critical factor for induced seismicity (e.g., Moeck et al., 2009; Pawley et al., 2018; Skoumal, Brudzinski, et al., 2018; Westwood et al., 2017). Although the lack of sufficient earthquake depth resolution prevents interpretation of where the seismicity is occurring, we note that carbonates like the Austin Chalk are more likely to produce induced seismicity than shales like the Eagle Ford (e.g., De Pater & Baisch, 2011; Lei et al., 2013; Sone & Zoback, 2014).

The largest earthquake during our study window was a M_L 3.5 (M_W 4.0; St. Louis University, 2018) on 1 May 2018 in Region 3 occurring within 3.25 km of two active well laterals (Figure 3a). This event was part of a sequence of earthquakes (92 events) that occurred within 10 km of two active well pads. Based on the spatiotemporal relationships between HF activity and the M_W 4.0 earthquake, this is potentially the largest HF-induced earthquake reported in the United States when compared with the M_L 3.5 (M_W 3.2) in Oklahoma (Skoumal, Ries, et al., 2018) and M_L 3.7 (M_W 3.4) in Ohio (Brudzinski & Kozłowska, 2019). The M_W 4.0 HF-induced event occurred ~10 km east of the largest earthquake recorded in the EF: a M_W 4.8

earthquake in October 2011 attributed to fluid extraction (Frohlich & Brunt, 2013). The best determined location of the October 2011 event (Frohlich & Brunt, 2013) is inside Region 2, in close proximity to sequences in Region 2 that reached M_L 3.4 (Figure 3c).

Within our enhanced earthquake catalog, there were $94 \geq M_L$ 2.0 and $10 \geq M_L$ 3.0 HF-induced earthquakes (supporting information, Table S3), and we calculated the Gutenberg–Richter b value to be 0.9 (Figure S8) (Caputo, 1976; Bender, 1983; Kijko & Smit, 2012; Wiemer & Wyss, 2000). Low b values (<1) and relatively large magnitudes are consistent with seismicity associated with fluid injection (Lei et al., 2008), whereas higher b values (~ 2) are typical of microseismicity ($M < 1$) directly related to the operational process of fracturing the reservoir (e.g., Wessels et al., 2011), suggesting the events we detected resulted from slip on pre-existing faults instead of new fractures. We did not undertake earthquake relocation due to the sparse station coverage at the time of this analysis, but a 2019 seismic deployment across the EF (<http://www.beg.utexas.edu/texnet>) is planned to enable this for future studies. Several earthquakes have TexNet fault plane solutions that show mostly normal slip on NE striking planes and a few strike slip (Figure 1). The trend of normal faults in this area and both types of fault plane solutions are consistent with NE-SW S_{HMAX} orientations (Lund Snee & Zoback, 2016), indicating faults in this area are optimally oriented for normal slip parallel to S_{HMIN} . This is consistent with previous findings that induced seismicity is most likely to occur on critically stressed faults that are well oriented in the present day stress field (e.g., Hennings et al., 2019; Moeck et al., 2009), mapped or not. The normal slip events we correlated with HF such as the M_W 4.0 event (Figure 1) are in contrast to pervasive strike-slip focal mechanisms reported for HF-induced seismicity in North America (e.g., Brudzinski & Kozłowska, 2019; Schultz et al., 2017), indicating HF-induced seismicity is not restricted to a particular fault type.

5. Stimulation Strategies and Probability of Seismicity

We identify three general timing patterns of well laterals, which we term simultaneous, sequential, and isolated. We defined laterals to be simultaneous if stimulation overlapped in time by at least half with another lateral on the pad (e.g., Figure 3b), sequential if stimulation occurred within 3 days of another lateral on the pad but overlapped in time by less than half (e.g., Figure 3d), and isolated if stimulation occurred more than 3 days from another lateral on the pad (e.g., supporting information, Figure S3e). Use of different overlap conditions from 25% to 75% changed the number of wells in a category by $<1\%$. Wells were defined to be on the same pad if the well heads were <100 m apart. Detailed stimulation reports are not publicly available, but all laterals are assumed to be completed in several dozen stages where portions of the horizontal wellbore are stimulated progressively from toe to heel. For simultaneous stimulation, the zipper method where stages alternate between laterals is the most likely pumping technique (Belyadi et al., 2016; Curnow & Tutuncu, 2016; Patel et al., 2016; Vermulen & Zoback, 2011).

We found 11.6% (71) of simultaneous, 6.9% (44) of sequential, and 3.9% (13) of isolated laterals produced seismicity (supporting information, Table S4). The largest event (M_W 4.0) occurred when two well pads were performing simultaneous lateral stimulations (Figure 3b). The odds ratio compared to an isolated lateral indicates seismicity was 3.2 \times more likely for a simultaneous lateral ($p = 0.0002$) and 1.8 \times more likely for a sequential lateral ($p = 0.06$). To assess what might be causing the different probabilities, we investigated several potential covariates. Wells for each stimulation strategy have a similar geographic distribution (supporting information, Figure S9), indicating that the probability differences are not due to regional variation. Larger HF injection volumes have been identified as a key influence on seismicity in Alberta, Canada (Schultz et al., 2018), and we found via logistic regression that there is a relationship between total volume injected into a lateral and probability of seismicity in our study ($p < 0.00001$, Figure 4a). We noted that sequential laterals have a slightly higher median volume than the other strategies (supporting information, Table S7). When we isolated our comparison of stimulation strategies to wells with a narrow range of total injected volumes (supporting information, Table S8), the odds ratios were similar for sequential and isolated wells, but the odds ratios remained larger ($\sim 4\times$) for simultaneous wells. We also examined the number of laterals on a well pad and logistic regression identified a relationship with the earthquake probability ($p < 0.00001$, Figure 4b). There is a difference in the mean number of laterals for isolated (1.2), simultaneous (2.5), and sequential (2.6), so we evaluated the probabilities for a narrow range of one to three laterals per

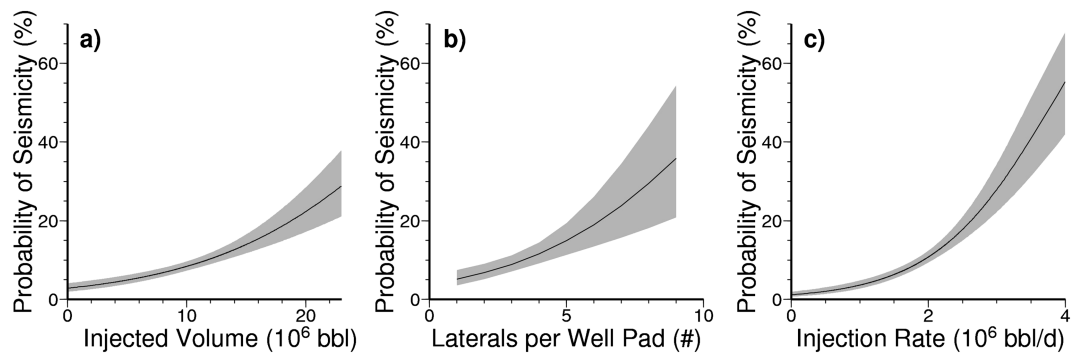


Figure 4. Predicted probability of seismicity from logistic regression for (a) injected volume, (b) number of laterals per well pad, and (c) daily effective injection rate. Line shows best fit and shading shows 95% confidence interval.

pad (supporting information, Table S9). We again found the probability for sequential and isolated are indistinguishable and restricting the number of laterals only lowers the odds ratio to 2.5× for simultaneous.

Our interpretation is that the primary reason why simultaneous laterals have a higher probability of seismicity is due to the higher overall injection rates over a comparable area. Note that this is an effective injection rate, as it is a weighted average between the actual injection rate during individual stages and the delay times between stages, with the latter likely more variable. The daily effective injection rate accounting for simultaneous laterals is strongly correlated with earthquake probability ($p < 0.00001$, Figure 4c). The mean effective injection rates (in 10^6 barrel per day) were 1.9, 1.5, and 1.2 for simultaneous, sequential, and isolated wells, respectively, with logistic regression predicting probabilities of 9.3%, 6.4%, and 4.5%, similar to what we observed (Table S4). This is consistent with recent mechanical modeling that found higher injection rates cause stronger poroelastic compression and higher pore fluid pressures resulting in a higher seismicity rate (Chang et al., 2018). In addition, extended pauses in injection between stages during sequential or isolated laterals (but not during zipper-type simultaneous laterals) would allow the poroelastic stresses to relax and the pore pressures to diffuse, contributing to the reduction in probability of seismicity. Yet when we restrict each of the stimulation categories to a narrow range of effective injection rate (volume per day, supporting information, Table S10), we still find a higher probability of seismicity for simultaneous wells, indicating that some other aspect of this strategy is also contributing to the higher probability. This is difficult to discern without detailed stimulation reports, but we acknowledge that simultaneous stimulation is inherently designed to cause stress interference and far field fracture complexity (e.g., Rafiee et al., 2012), and the higher pressures may promote aseismic slip that is proposed to drive HF-induced seismicity by outpacing the pore pressure diffusion front (Eyre et al., 2019). So, while there are economic advantages to simultaneous stimulation through faster injection that reduces time on the well pad and potentially more stimulated reservoir, the increased effective injection rate results in an increased probability of seismicity.

6. Conclusions and Implications on Operations

This study identified that the seismicity rate in the EF has grown rapidly since 2014 and that most of the earthquakes are spatiotemporally correlated with HF. Currently, there are no regulations that address seismicity caused by HF in Texas, so to place this activity in context, we compare the seismicity to traffic light protocols in other areas of North America. The green light, where no action is necessary is $M < 1.5$ in Ohio and $M < 2$ in Oklahoma and Alberta; the yellow light typically involves implementing a response plan and extends to $M < 2.5$ in Ohio, $M < 3$ in Oklahoma, and $M < 4$ in Alberta; and the red light results in pad suspension at $M \geq 3$ in Ohio, $M \geq 3.5$ in Oklahoma, and $M \geq 4$ in Alberta (Alberta Energy Regulator, 2015; Ohio Department of Natural Resources, 2017; Oklahoma Corporation Commission, 2018). If a similar protocol had been implemented in Texas, as many as 178 wells would have been above a yellow light threshold and 69 above a red light (Table S3). The majority of these cases occurred in 2018 due to the increasing rate and magnitude of seismicity, including one of the largest documented HF-induced earthquakes in the United States ($M_w 4.0$). Mapped faults in this area appear capable of hosting larger events, as HF has been shown to induce larger magnitude events in

Canada (Mahani et al., 2017) and China (Lei et al., 2019). Our results indicate that key influences on probability of HF-induced seismicity are proximity to faults, orientation of faults in the stress field, effective injection rate, injected volume, and number of laterals on a well pad.

Acknowledgments

Acknowledgements This work was supported by NSF Grant 1614942 and U.S. Geological Survey NEHRP Grant 2018-0184. We thank C. Cooper, P. Hennings, D. Huang, A. Morris, J. Nunn, R. Ries, A. Rios, A. Savvaidis, T. Tyrrell, and A. Velasco for their insightful discussions which benefited this study. We thank editor H. Rajaram, and reviewers A. Barbour, E. Cochran, M. Diggles, S. Hecker, O. Kaven, R. Schultz, and D. Trugman. The initial catalog of earthquakes was obtained from TexNet (<http://www.beg.utexas.edu/texnet>). Seismic waveform data from the N4 (<https://doi.org/10.7914/SN/N4>) and TA (<https://doi.org/10.7914/SN/TA>) seismic networks were obtained from the Incorporated Research Institutions for Seismology Data Management Center (<http://service.iris.edu/fdsnws>). HF data were retrieved from FracFocus (<http://fracfocus.org/>) and WD from the Railroad Commission of Texas (<http://webapps.rrc.texas.gov/H10/searchVolume.do>).

References

- Alberta Energy Regulator (AER) (2015). Subsurface order no. 2: Monitoring and reporting of seismicity in the vicinity of hydraulic fracturing operations in the Duvernay zone, Fox Creek, Alberta. AER Bulletin 2015-07, 3 pp., <https://aer.ca/documents/orders/subsur-face-orders/SO2.pdf>, Accessed July 2017.
- Altman, D. G. (1991). *Practical statistics for medical research*. London: Chapman and Hall.
- Atkinson, G. M., Eaton, D. W., Ghofrani, H., Walker, D., Cheadle, B., Schultz, R., et al. (2016). Hydraulic fracturing and seismicity in the western Canada sedimentary basin. *Seismological Research Letters*, 87(3), 631–647. <https://doi.org/10.1785/0220150263>
- Belyadi, H., Fathi, E., & Belyadi, F. (2016). *Hydraulic fracturing in unconventional reservoirs: Theories, operations, and economic analysis* (p. 453). Cambridge, MA: Gulf Professional Publishing.
- Bender, B. (1983). Maximum likelihood estimation of b values for magnitude grouped data. *Bulletin of the Seismological Society of America*, 73(3), 831–851.
- Brudzinski, M. R., & Kozlowska, M. (2019). Seismicity induced by hydraulic fracturing and wastewater disposal in the Appalachian Basin, USA: A review. *Acta Geophysica*, 67(1), 351–364. <https://doi.org/10.1007/s11600-019-00249-7>
- Caputo, M. (1976). Model and observed seismicity represented in a two dimensional space. *Annals of Geophysics*, 29(4), 277–288.
- Chang, K. W., Yoon, H., & Martinez, M. J. (2018). Seismicity rate surge on faults after shut-in: Poroelastic response to fluid injection. *Bulletin of the Seismological Society of America*, 108(4), 1889–1904. <https://doi.org/10.1785/0120180054>
- Clarke, H., Eisner, L., Styles, P., & Turner, P. (2014). Felt seismicity associated with shale gas hydraulic fracturing: The first documented example in Europe. *Geophysical Research Letters*, 41, 8308–8314. <https://doi.org/10.1002/2014GL062047>
- Curnow, J. S., & Tutuncu, A. N. (2016). A coupled geomechanics and fluid flow modeling study for hydraulic fracture design and production optimization in an eagle ford shale oil reservoir. Paper presented at SPE Hydraulic Fracturing Technology Conference. Society of Petroleum Engineers. The Woodlands, Tex. <https://doi.org/10.2118/179165-MS>
- Davis, S. D., Nyffenegger, P. A., & Froehlich, C. (1995). The 9 April 1993 earthquake in south-central Texas: Was it induced by fluid withdrawal? *Bulletin of the Seismological Society of America*, 85(6), 1888–1895.
- De Pater, C. J., & Baisch, S. (2011). Geomechanical study of Bowland Shale seismicity. *Synth. Rep*, 71.
- EIA. (2019). Drilling productivity report: For key tight oil and shale gas regions. <https://www.eia.gov/petroleum/drilling/>.
- Ellsworth, W. L. (2013). Injection-induced earthquakes. *Science*, 341(6142), 1225942. <https://doi.org/10.1126/science.1225942>
- Ewing, T. E. (1990). Tectonic map of Texas (scale 1: 750,000). Austin, Tex: University of Texas Bureau of Economic Geology.
- Eyre, T. S., Eaton, D. W., Garagash, D. I., Zecovic, M., Venieri, M., Weir, R., & Lawton, D. C. (2019). The role of aseismic slip in hydraulic fracturing-induced seismicity. *Science Advances*, 5(8), eaav7172. <http://doi.org/10.1126/sciadv.aav7172>
- Farahbod, A. M., Kao, H., Walker, D. M., & Cassidy, J. F. (2015). Investigation of regional seismicity before and after hydraulic fracturing in the Horn River Basin, northeast British Columbia. *Canadian Journal of Earth Sciences*, 52(2), 112–122. <https://doi.org/10.1139/cjes-2014-0162>
- Froehlich, C., & Brunt, M. (2013). Two-year survey of earthquakes and injection/production wells in the Eagle Ford Shale, Texas, prior to the M_w 4.8 20 October 2011 earthquake. *Earth and Planetary Science Letters*, 379, 56–63. <https://doi.org/10.1016/j.epsl.2013.07.025>
- Froehlich, C., & Davis, S. D. (2002). *Texas earthquakes* (Vol. 2, p. 275). Austin, Tex: University of Texas Press.
- Froehlich, C., DeShon, H., Stump, B., Hayward, C., Hornbach, M., & Walter, J. I. (2016). A historical review of induced earthquakes in Texas. *Seismological Research Letters*, 87(4), 1022–1038. <https://doi.org/10.1785/0220160016>
- Haffener, J., Chen, X., & Murray, K. (2018). Multiscale analysis of spatiotemporal relationship between injection and seismicity in Oklahoma. *Journal of Geophysical Research: Solid Earth*, 123, 8711–8731. <https://doi.org/10.1029/2018JB015512>
- Hennings, P. H., Lund Snee, J. E., Osmond, J. L., DeShon, H. R., Dommis, R., Horne, E., et al. (2019). Injection-induced seismicity and fault-slip potential in the Fort Worth Basin, Texas. *Bulletin of the Seismological Society of America*, 109(5), 1615–1634. <https://doi.org/10.1785/0120190017>
- IRIS Transportable Array (2003). USArray transportable array. International Federation of Digital Seismograph Networks. Dataset/Seismic Network. <https://doi.org/10.7914/SN/TA>
- Johnson, L. R. (2014). Source mechanisms of induced earthquakes at The Geysers geothermal reservoir. *Pure and Applied Geophysics*, 171(8), 1641–1668. <https://doi.org/10.1007/s00024-014-0795-x>
- Kaven, J. O., Hickman, S. H., McGarr, A. F., & Ellsworth, W. L. (2015). Surface monitoring of microseismicity at the Decatur, Illinois, CO₂ sequestration demonstration site. *Seismological Research Letters*, 86(4), 1096–1101. <https://doi.org/10.1785/0220150062>
- Keranen, K. M., Savage, H. M., Abers, G. A., & Cochran, E. S. (2013). Potentially induced earthquakes in Oklahoma, USA: Links between wastewater injection and the 2011 M_w 5.7 earthquake sequence. *Geology*, 41(6), 699–702. <https://doi.org/10.1130/G34045.1>
- Keranen, K. M., & Weingarten, M. (2018). Induced seismicity. *Annual Review of Earth and Planetary Sciences*, 46, 149–174. <https://doi.org/10.1146/annurev-earth-082517-010054>
- Kijko, A., & Smit, A. (2012). Extension of the Aki-Utsu b-value estimator for incomplete catalogs. *Bulletin of the Seismological Society of America*, 102(3), 1283–1287. <https://doi.org/10.1785/0120110226>
- Kozlowska, M., Brudzinski, M. R., Friberg, P., Skoumal, R. J., Baxter, N. D., & Currie, B. S. (2018). Maturity of nearby faults influences seismic hazard from hydraulic fracturing. *Proceedings of the National Academy of Sciences*, 115(8), E1720–E1729. <https://doi.org/10.1073/pnas.1715284115>
- Lei, X., Huang, D., Su, J., Jiang, G., Wang, X., Wang, H., et al. (2017). Fault reactivation and earthquakes with magnitudes of up to M_w 4.7 induced by shale-gas hydraulic fracturing in Sichuan Basin, China. *Scientific Reports*, 7(1), 7971. <https://doi.org/10.1038/s41598-017-08557-y>
- Lei, X., Ma, S., Chen, W., Pang, C., Zeng, J., & Jiang, B. (2013). A detailed view of the injection-induced seismicity in a natural gas reservoir in Zigong, southwestern Sichuan basin, China. *Journal of Geophysical Research: Solid Earth*, 118, 4296–4311. <https://doi.org/10.1002/jgrb.50310>
- Lei, X., Wang, Z., & Su, J. (2019). The December 2018 M_L 5.7 and January 2019 M_L 5.3 earthquakes in South Sichuan basin induced by shale gas hydraulic fracturing. *Seismological Research Letters*, 90(3), 1099–1110. <https://doi.org/10.1785/0220190029>

- Lei, X., Yu, G., Ma, S., Wen, X., & Wang, Q. (2008). Earthquakes induced by water injection at ~3 km depth within the Rongchang gas field, Chongqing, China. *Journal of Geophysical Research*, 113, B10310. <https://doi.org/10.1029/2008JB005604>
- Lund Snee, J. E., & Zoback, M. D. (2016). State of stress in Texas: Implications for induced seismicity. *Geophysical Research Letters*, 43, 10,208–10,214. <https://doi.org/10.1002/2016GL070974>
- Mahani, A. B., Schultz, R., Kao, H., Walker, D., Johnson, J., & Salas, C. (2017). Fluid injection and seismic activity in the northern Montney play, British Columbia, Canada, with special reference to the 17 August 2015 M_w 4.6 induced earthquake. *Bulletin of the Seismological Society of America*, 107(2), 542–552. <https://doi.org/10.1785/0120160175>
- Martin, R., Baily, J. D., Malpani, R., Lindsay, G. J., & Atwood, W. K. (2011). Understanding production from Eagle Ford-Austin chalk system. Paper presented at SPE Annual Technical Conference and Exhibition. Society of Petroleum Engineers. Denver, Col. <https://doi.org/10.2118/145117-MS>
- McGarr, A. (2014). Maximum magnitude earthquakes induced by fluid injection. *Journal of Geophysical Research: Solid Earth*, 119, 1008–1019. <https://doi.org/10.1002/2013JB010597>
- Moeck, I., Kwiatek, G., & Zimmermann, G. (2009). Slip tendency analysis, fault reactivation potential and induced seismicity in a deep geothermal reservoir. *Journal of Structural Geology*, 31(10), 1174–1182. <https://doi.org/10.1016/j.jsg.2009.06.012>
- National Research Council (2013). *Induced seismicity potential in energy technologies*. Washington, DC: National Academies Press. <https://doi.org/10.17226/13355>
- Ohio Department of Natural Resources (ODNR) (2017). Division of oil and gas resources management, AGI policy & critical issues webinar: OhioNET: State of Ohio's response to induced seismicity. April 14 2017.
- Oklahoma Corporation Commission (OCC) (2018). Moving forward: New protocol to further address seismicity in state's largest oil and gas play [Press release], <https://www.occeweb.com/og/02-27-18PROTOCOL.pdf>.
- Olson, D. R., & Frohlich, C. (1992). Research note: Felt reports from the 20 July 1991 Falls City Earthquake, Karnes County, Texas. *Seismological Research Letters*, 63(4), 603–604. <https://doi.org/10.1785/gssrl.63.4.603>
- Patel, H., Cadwallader, S., & Wampler, J. (2016). Zipper fracturing: Taking theory to reality in the Eagle Ford Shale. Paper presented at Unconventional Resources Technology Conference (pp. 1000–1008). Society of Exploration Geophysicists, American Association of Petroleum Geologists, Society of Petroleum Engineers. San Antonio, Tex. <https://doi.org/10.15530/urtec-2016-2445923>
- Pawley, S., Schultz, R., Playter, T., Corlett, H., Shipman, T., Lyster, S., & Hauck, T. (2018). The geological susceptibility of induced earthquakes in the Duvernay play. *Geophysical Research Letters*, 45, 1786–1793. <https://doi.org/10.1002/2017GL076100>
- Pearson, K. (2012). Geologic models and evaluation of undiscovered conventional and continuous oil and gas resources—Upper Cretaceous Austin Chalk. *U.S. Gulf Coast: U.S. Geological Survey Scientific Investigations Report 2012-5159*, 26, <https://doi.org/10.3133/sir20125159>.
- Pennington, W. D., Davis, S. D., Carlson, S. M., DuPree, J., & Ewing, T. E. (1986). The evolution of seismic barriers and asperities caused by the depressuring of fault planes in oil and gas fields of south Texas. *Bulletin of the Seismological Society of America*, 76(4), 939–948.
- Rafiee, M., Soliman, M. Y., & Pirayesh, E. (2012). Hydraulic fracturing design and optimization: A modification to zipper frac. Paper presented at SPE Annual Technical Conference and Exhibition. Society of Petroleum Engineers. San Antonio, Tex. <https://doi.org/10.2118/159786-MS>
- Railroad Commission of Texas (RRC) (2019). Texas Eagle Ford Shale oil production 2008 through March 2019. <https://www.rrc.state.tx.us/media/52456/eagle-ford-oil.pdf>.
- Rubinstein, J. L., & Mahani, A. B. (2015). Myths and facts on wastewater injection, hydraulic fracturing, enhanced oil recovery, and induced seismicity. *Seismological Research Letters*, 86(4), 1060–1067. <https://doi.org/10.1785/0220150067>
- Schaff, D. P., & Richards, P. G. (2014). Improvements in magnitude precision, using the statistics of relative amplitudes measured by cross correlation. *Geophysical Journal International*, 197(1), 335–350. <https://doi.org/10.1093/gji/ggt433>
- Schultz, R., Atkinson, G., Eaton, D. W., Gu, Y. J., & Kao, H. (2018). Hydraulic fracturing volume is associated with induced earthquake productivity in the Duvernay play. *Science*, 359(6373), 304–308. <https://doi.org/10.1126/science.aa0159>
- Schultz, R., Wang, R., Gu, Y. J., Haug, K., & Atkinson, G. (2017). A seismological overview of the induced earthquakes in the Duvernay play near Fox Creek, Alberta. *Journal of Geophysical Research: Solid Earth*, 122, 492–505. <https://doi.org/10.1002/2016JB013570>
- Segall, P., & Lu, S. (2015). Injection-induced seismicity: Poroelastic and earthquake nucleation effects. *Journal of Geophysical Research: Solid Earth*, 120, 5082–5103. <https://doi.org/10.1002/2015JB012060>
- Sheskin, D. J. (2004). *Handbook of parametric and nonparametric statistical procedures*, (3rd ed.). Boca Raton: Chapman & Hall/CRC.
- Skoumal, R. J., Brudzinski, M. R., & Currie, B. S. (2015). Earthquakes induced by hydraulic fracturing in Poland Township, Ohio. *Bulletin of the Seismological Society of America*, 105(1), 189–197. <https://doi.org/10.1785/0120140168>
- Skoumal, R. J., Brudzinski, M. R., & Currie, B. S. (2018). Proximity of Precambrian basement affects the likelihood of induced seismicity in the Appalachian, Illinois, and Williston Basins, central and eastern United States. *Geosphere*, 14(3), 1365–1379. <https://doi.org/10.1130/GES01542>
- Skoumal, R. J., Brudzinski, M. R., Currie, B. S., & Levy, J. (2014). Optimizing multi-station earthquake template matching through re-examination of the Youngstown, Ohio, sequence. *Earth and Planetary Science Letters*, 405, 274–280. <https://doi.org/10.1016/j.epsl.2014.08.033>
- Skoumal, R. J., Kaven, J. O., & Walter, J. I. (2019). Characterizing seismogenic fault structures in Oklahoma using a relocated template-matched catalog. *Seismological Research Letters*, 90(4), 1535–1543. <https://doi.org/10.1785/0220190045>
- Skoumal, R. J., Ries, R., Brudzinski, M. R., Barbour, A. J., & Currie, B. S. (2018). Earthquakes induced by hydraulic fracturing are pervasive in Oklahoma. *Journal of Geophysical Research: Solid Earth*, 123, 10,918–10,935. <https://doi.org/10.1029/2018JB016790>
- Sone, H., & Zoback, M. D. (2014). Time-dependent deformation of shale gas reservoir rocks and its long-term effect on the in situ state of stress. *International Journal of Rock Mechanics and Mining Sciences*, 69, 120–132. <https://doi.org/10.1016/j.ijrmms.2014.04.002>
- St. Louis University (SLU) (2018). 20180501162854 Focal mechanism. http://www.eas.slu.edu/eqc/eqc_mt/MECH.NA/20180501162854
- UC San Diego (2013). Central and eastern U.S. Network, International Federation of Digital Seismograph Networks, Dataset/Seismic Network. <https://doi.org/10.7914/SN/N4>
- Vermylen, J., & Zoback, M. D. (2011). Hydraulic fracturing, microseismic magnitudes, and stress evolution in the Barnett Shale, Texas, USA. Paper presented at SPE Hydraulic Fracturing Technology Conference. Society of Petroleum Engineers. The Woodlands, Tex. <https://doi.org/10.2118/140507-MS>
- Walsh, F. R., & Zoback, M. D. (2015). Oklahoma's recent earthquakes and saltwater disposal. *Science Advances*, 1(5), e1500195. <https://doi.org/10.1126/sciadv.1500195>
- Walsh, F. R., & Zoback, M. D. (2016). Probabilistic assessment of potential fault slip related to injection-induced earthquakes: Application to north-central Oklahoma, USA. *Geology*, 44(12), 991–994. <https://doi.org/10.1130/G38275.1>

- Walter, J. I., Chang, J. C., & Dotray, P. J. (2017). Foreshock seismicity suggests gradual differential stress increase in the months prior to the 3 September 2016 M_w 5.8 Pawnee earthquake. *Seismological Research Letters*, 88(4), 1032–1039. <https://doi.org/10.1785/0220170007>
- Walter, J. I., Frohlich, C., & Borgfeldt, T. (2018). Natural and induced seismicity in the Texas and Oklahoma Panhandles. *Seismological Research Letters*, 89(6), 2437–2446. <https://doi.org/10.1785/0220180105>
- Warpinski, N. R., Du, J., & Zimmer, U. (2012). Measurements of hydraulic-fracture-induced seismicity in gas shales. *SPE Production & Operations*, 27(03), 240–252. <https://doi.org/10.2118/151597-PA>
- Weingarten, M., Ge, S., Godt, J. W., Bekins, B. A., & Rubinstein, J. L. (2015). High-rate injection is associated with the increase in US mid-continent seismicity. *Science*, 348(6241), 1336–1340. <https://doi.org/10.1126/science.aab1345>
- Wessels, S. A., De La Pena, A., Kratz, M., Williams-Stroud, S., & Jbeili, T. (2011). Identifying faults and fractures in unconventional reservoirs through microseismic monitoring. *First Break*, 29(7), 99–104.
- Westwood, R. F., Toon, S. M., Styles, P., & Cassidy, N. J. (2017). Horizontal respect distance for hydraulic fracturing in the vicinity of existing faults in deep geological reservoirs: A review and modelling study. *Geomechanics and Geophysics for Geo-energy and Georesources*, 3(4), 379–391. <https://doi.org/10.1007/s40948-017-0065-3>
- Wiemer, S., & Wyss, M. (2000). Minimum magnitude of completeness in earthquake catalogs: Examples from Alaska, the western United States, and Japan. *Bulletin of the Seismological Society of America*, 90(4), 859–869. <https://doi.org/10.1785/0119990114>
- Yeck, W. L., Hayes, G. P., McNamara, D. E., Rubinstein, J. L., Barnhart, W. D., Earle, P. S., & Benz, H. M. (2017). Oklahoma experiences largest earthquake during ongoing regional wastewater injection hazard mitigation efforts. *Geophysical Research Letters*, 44, 711–717. <https://doi.org/10.1002/2016GL071685>
- Yoon, C. E., Huang, Y., Ellsworth, W. L., & Beroza, G. C. (2017). Seismicity during the initial stages of the Guy-Greenbrier, Arkansas, earthquake sequence. *Journal of Geophysical Research: Solid Earth*, 122, 9253–9274. <https://doi.org/10.1002/2017JB014946>